Direct Force Measurements of Insulin Monomer−Monomer Interactions†

Christopher M. Yip,*,‡,§ Cecil C. Yip,|| and Michael D. Ward*,‡

Department of Chemical Engineering and Materials Science, University of Minnesota, Minneapolis, Minnesota 55455, and Banting and Best Department of Medical Research, University of Toronto, Toronto, Ontario M5G 1L6, Canada

Received September 11, 1997; Revised Manuscript Received November 25, 1997

ABSTRACT: Direct measurement of the forces involved in protein−protein and protein−receptor interactions can, in principle, provide insight necessary for the advancement of structural biology, molecular biology, and the development of therapeutic proteins. The protein insulin is illustrative in this respect as the mechanisms of insulin dimer dissociation and insulin−insulin receptor binding are crucial to the efficacy of insulin medications for the control of diabetes. Insulin molecules, modified with a photochemically active azido functionality on specific residues, were attached to force microscope tips and opposing mica surfaces in configurations that would either favor or disfavor dimer formation. Force curve measurements performed in buffer solution revealed the complexity of the insulin monomer−monomer interaction with multiple unbinding events occurring upon tip retraction, suggesting disruption of discrete molecular bonds at the monomer−monomer interface. Furthermore, the force curves exhibit long-range unbinding events, consistent with considerable elongation of the insulin molecule prior to dissociation. The unbinding forces observed in this study are the result of a combination of molecular disentanglement and dimer dissociation processes.

Insulin, a 5800 Da protein comprising a 21 amino acid A chain and a 30 amino acid B chain linked by two disulfide bridges, is stored in the pancreatic β cells in a hexameric form (Figure 1A). However, it interacts as a monomer with its transmembrane receptor to increase glucose transport and utilization. The efficacy of insulin formulations for the treatment of insulin-dependent diabetes therefore greatly depends on a better understanding of insulin association and dissociation and of the influence of directed mutations and specific binding agents on these processes. A key step toward this goal would be the direct and convenient measurement of protein binding forces associated with insulin dimer formation, which represents a key intermediate stage of dissociation.

Recently, surface forces (*1*), optical tweezers (*2*), interfacial force microscopy (IFM) (*3*), atomic force microscopy (AFM)[1] (*4*), and micropipet techniques (*5*) have been employed to probe directly various intermolecular and ligand−receptor binding interactions. Surface mapping of spatially heterogeneous adhesion and friction due to segregated functional groups has been accomplished by using chemically modified AFM tips (*6*−*9*). Of particular relevance to the present work, AFM has been used to study the adhesive strength and mechanics of various biomolecular binding interactions, including antibody−antigen (*10*), ferritin−anti-ferritin antibody, (*11*), streptavidin−biotin (*12*−*14*), and DNA−nucleotide adhesive interactions (*15*). These measurements rely on measurement of the deflection of an AFM cantilever, with a known force constant, during retraction of a sample surface from an appropriately modified AFM tip. In addition to elucidating specific molecular recognition events, further advancement of these techniques may lead to imaging of the distribution of specific binding sites on bioactive membrane surfaces, as well as improvements in the topographic images of such surfaces.

To measure the forces associated with protein−protein or protein−ligand binding, the relevant species must be attached to opposing surfaces (i.e., an AFM tip and a sample surface) in an orientation that favors approach of the active binding sites. The existence of three distinct antibody−antigen binding geometries (cavity, groove, and planar) suggests that the physical structure presented at the protein interface will influence binding forces and affinities significantly (*16*). Therefore, the immobilization procedure should be designed so that the native protein conformation is not disturbed substantially in order that the system mimics solution behavior as closely as possible. Indeed, studies have

† This work was supported by National Science Foundation Grant DMR-9408923 and Office of Naval Research Grant N00014-93-1-0563 (M.D.W.), and Medical Research Council of Canada Grant 8947 (C.C.Y.).

* Correspondence should be directed to either of these authors. C.M.Y.: Institute of Biomedical Engineering, University of Toronto, 4 Taddle Creek Rd., Toronto, Ontario, Canada M5S 3G9; Tel (416) 978-7853; Fax (416) 978-4317. E-mail yip@ibme.utoronto.ca. M.D.W.: Department of Chemical Engineering and Materials Science, University of Minnesota, Amundson Hall, 421 Washington Ave. SE, Minneapolis, MN 55455; Tel (612) 625-3062; Fax (612) 626-7246; E-mail wardx004@maroon.tc.umn.edu.

‡ Department of Chemical Engineering and Materials Science,University of Minnesota.

§ Present address: Institute of Biomedical Engineering, University of Toronto M5S 3G9.

|| Banting and Best Department of Medical Research, University of Toronto.

[1] Abbreviations: **B29**-MABI, ($N^{\epsilon B29}$-monoazidobenzoyl)insulin; **B1**-MABI, ($N^{\alpha B1}$-monoazidobenzoyl)insulin; PBS, phosphate-buffered saline; AFM, atomic force microscopy; MAb 21, monoclonal anti-insulin antibody; N-IgG, normal guinea pig immunoglobulin γ G; 3-APTES, (3-aminopropyl)triethoxysilane.

S0006-2960(97)02275-7 CCC: $15.00
Published on Web 04/02/1998

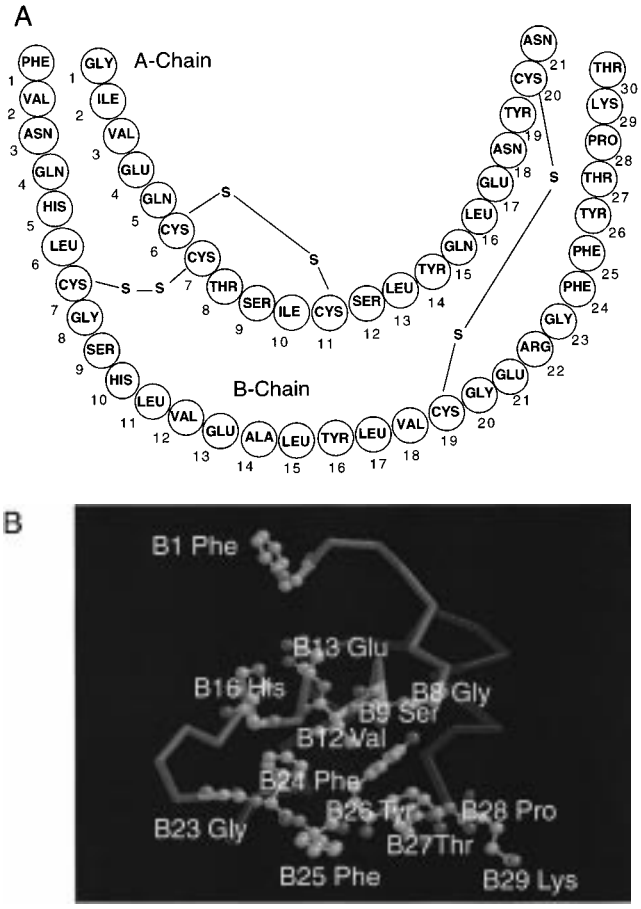

FIGURE 1: (A) Sequence for human insulin, illustrating the A and B chains. Disulfide links between the A7 Cys and B7 Cys and A20 Cys and B17 Cys enforce the conformation of this portion of the insulin molecule. (B) Molecular model of the insulin monomer based on a structure deduced from NMR studies of a B16 Tyr → His mutant insulin. The model is oriented to reveal the binding domain comprising B8 Gly, B9 Ser, B12 Val, B13 Gln, B16 Tyr (here replaced with His), B23 Gly, B24 Phe, B25 Phe, B26 Tyr, B27 Thr, and B28 Pro. The insulin molecule is drawn as a backbone model with the A and B chains depicted in blue and red, respectively. Those residues involved in dimer formation as well as the immobilization sites B1 Phe and B29 Lys are depicted as ball-and-stick models. The model was prepared with RasMol v 2.6 using coordinates deposited in the Brookhaven Protein Data Bank under entry code pdb1hls.

demonstrated that several proteins, such as insulin, growth hormone, RGDS tetrapeptide fragments, and interleukin 2, can remain bioactive upon surface immobilization provided the immobilized protein is oriented properly or has sufficient conformational flexibility (*17*, *18*).

While measurements of streptavidin−biotin binding forces have exploited the 222-point symmetry of the streptavidin tetramer, which is nearly ideal for attachment of the protein to surfaces and subsequent measurement of ligand−receptor binding (*19*−*21*), such fortuitous symmetry and arrangement of binding sites is not evident in the insulin molecule, whose dimerization interface is substantially more complex than the streptavidin−biotin binding site. Crystallographic studies have revealed that the residues responsible for insulin dimer formation are located primarily in the B chain, including B8 Gly, B9 Ser, B12 Val, B13 Glu, B16 Tyr, B23 Gly, B24 Phe, B25 Phe, B26 Tyr, B27 Thr, and B28 Pro (Figure 1B) (*22*) (Table 1). Many of these same residues also have been implicated in insulin receptor binding (as reviewed in refs

Table 1: Insulin Monomer−Monomer Contacts[a]

B8-Gly	B8-Gly
B9-Ser	B9-Ser
B12-Val	B12-Val
B13-Glu	B13-Glu
B16-Tyr	B16-Tyr
B23-Gly	B23-Gly
B24-Phe	B24-Phe
B25 Tyr	B25 Tyr
B26-Tyr	B26-Tyr
B27-Thr	B27-Thr

[a] Adapted from ref 25.

23 and *24*). Residues B24 through B26 adopt a β-sheet structure, with the dimer-forming interface defined by contact between these nominally planar β-sheets arranged in an antiparallel fashion. The prominent intermonomer interactions in this region are hydrogen bonds between B24 Phe and B26 Tyr of each monomer (*25*). These interactions conspire to make insulin dimer formation favorable as indicated by the moderate association constants reported for this process, which range from 7.7×10^3 to 7.5×10^5 M^{-1} (*26*).

To identify possible tethering points on the insulin molecule, it is necessary to examine the solution conformation of the insulin monomer. However, insulin's complex self-association characteristics have hampered such determinations based on native insulins, and while it is possible to infer a solution conformation from analyses of X-ray crystal structures, this can be complicated by crystal packing forces. Accordingly, we based our model on the high-resolution (average rms backbone deviation 0.89 Å) solution NMR structure reported for B16 Tyr → His mutant of human insulin (Brookhaven Protein Data Bank entry code 1hls.ent) (*27*). This mutant insulin is particularly well-suited for our purposes as it exists as a monomer in solution and has only a single-site mutation compared to other monomeric insulins that typically bear large sequence deletions. Remarkably, the solution conformation of this mutant insulin is comparable to that adopted by monomer 1 in the 2Zn insulin hexamer crystal structure (*24*). Close inspection of the NMR model suggested that attachment of an insulin monomer to a surface via the B1 Phe residue, located at the N-terminus of the B chain, would direct the dimer forming domain away from the surface. Conversely, immobilization via the B29 Lys residue, located near the C-terminus of the B chain, would pin the binding domain at the surface. Further evidence for exposure of the dimerization domains upon immobilization via B1 Phe can be seen in the following. Photoaffinity labeling studies determined that the B29 Lys residue lies immediately adjacent to the receptor binding domain with the B1 Phe terminus located distal to this region,

which suggests that both the receptor binding and dimerization domains would be exposed upon surface immobilization via B1 Phe (*28*). This is supported by a study that demonstrated that insulin covalently bound to surface-hydrolyzed poly(methyl methacrylate) films under conditions favoring attachment via B1 Phe was capable of stimulating Chinese hamster ovary cell growth (*17*). These observations are consistent with exposure of the receptor-binding and, by inference, dimer-forming domains of the B1 Phe-immobilized insulin molecules. Therefore, we postulated that these two orientations would exhibit different force characteristics associated with the relative accessibility of the dimer-forming domains.

Herein we report in situ AFM-based measurements of the adhesion force between insulin monomers whose orientation on the AFM tip and an opposing mica surface are dictated by photochemical attachment of specific residues to these surfaces. The measurements reveal that the binding characteristics differ substantially for differently oriented monomers and that dimerization adhesive forces are influenced by binding antagonists such as free insulin and anti-insulin antibodies. The force curves exhibit long-range unbinding events, consistent with considerable insulin extensibility as the dimerized monomers are pulled apart. The force curves are nominally identical for repeated measurements, indicating reversible and rapid refolding of the protein. These results suggest a protocol for evaluating the effects of antagonists and sequence alterations on insulin dimer formation and measuring insulin−receptor interactions, which could have significant impact on the development of therapeutic formulations for the treatment of diabetes.

MATERIALS AND METHODS

Photoreactive Insulin Derivatives. The photoreactive ($N^{\epsilon\mathbf{B29}}$-monoazidobenzoyl)insulin (**B29**-MABI) and ($N^{\alpha\mathbf{B1}}$-monoazidobenzoyl)insulin (**B1**-MABI) were prepared from bovine insulin as described previously (*28*). These derivatives possess a photochemically active azido group on the B29 Lys or B1 Phe residue, respectively, that enables covalent coupling of these residues to the exposed amine functionalities of the modified surfaces. The lyophilized reagents were stored in the dark at −20 °C until required for use. Aliquots were reconstituted at a concentration of ∼0.025 mg/mL (∼4 μM). The **B29**-MABI solution was prepared in 0.2 M Na_2HPO_4/NaH_2PO_4 and 0.9% NaCl, while **B1**-MABI was reconstituted using 0.006 N HCl.

Surface Immobilization of Insulin on Mica and AFM Tips. Freshly cleaved mica was immersed in a 2% (w/w) acetone solution of (3-aminopropyl)triethoxysilane (Aldrich, Milwaukee, WI), which reacts with surface -OH groups and introduces reactive-NH_2 groups to these surfaces (*29*), for 1 h, rinsed extensively with anhydrous acetone, and cured at 49 °C for approximately 1 h. The aminosilane-modified mica was photolabeled with the photoreactive insulin by placing ∼150 μL of the reagent solution on the mica surface and irradiating it for 1 h with ultraviolet light (354 nm). In separate experiments we established that the photoreactive insulin derivatives remained fully biologically active after exposure to ultraviolet irradiation as demonstrated by their binding to the insulin receptor (data not shown). After irradiation, the insulin-modified mica was rinsed sequentially with copious amounts of pH 7.5 phosphate-buffered saline (PBS) solution and pH 3.5 glycine buffer to remove any of the insulin derivatives not covalently attached to the mica. The insulin concentrations (∼4 μM) employed during immobilization were sufficiently low to preclude significant populations of insulin dimers. While we cannot conclusively prove that such species are not present, we expect that the rinsing procedure performed under acidic conditions (pH 3.5 glycine buffer) would remove most if not all noncovalent insulin dimers. After a final rinse with pH 7.5 PBS solution, the derivatized mica was stored at 4 °C in PBS solution until use. Pyramidal Si_4N_3 AFM tips (Digital Instruments, Inc., type DNP) were modified and stored in an identical fashion. Although the Si_4N_3 surface of the AFM tip possesses low concentrations of native -NH_2 functionalities (*30*) that may be sufficient for attachment of photoactive insulin derivatives, the tips were treated with 3-APTES in order to increase the surface density of active -NH_2 groups (Figure 2). Similar tip modification schemes have been employed by others (*31*).

Other Reagents. Monoclonal anti-insulin (MAb 21) and normal guinea pig immunoglobulin γ G (N-IgG) were prepared as previously described (*32*, *33*). Stock 0.158 mg/mL N-IgG solution was prepared in pH 7.5 PBS buffer solution and diluted 100-fold in pH 7.5 PBS buffer. The lyophilized MAb 21 was reconstituted in pH 7.5 PBS buffer solution to a nominal concentration of ∼1 μg/mL. Bovine insulin (Sigma) was used as received. Stock bovine insulin solutions at concentrations ranging from 10 to 1 μg/mL were prepared from pH 3.5 glycine buffer solutions and stored at 4 °C until needed.

Atomic Force Microscopy. All AFM data were obtained on a NanoScope III MultiMode scanning probe microscope (Digital Instruments, Inc., Santa Barbara, CA) equipped with 200 μm V-shaped Si_3N_4 cantilevers. Images were analyzed with the Digital Instruments Nanoscope III version 4.22 software. The vertical dimensions of insulin molecules that had been photochemically attached to the mica surface were determined on arbitrarily selected regions of the image using the threshold feature, with a threshold height of 0 nm. The average feature height was determined from the average peak height above the threshold value. The baseline, which corresponded to the threshold height, was chosen by a first-order plane fit to the image region.

Force curves were obtained by disabling the $x-y$ scanning motion and modulating the z-axis-directed piezo motion. Complete force curves were acquired within 2−10 s. Contact forces were kept below 2 nN in order to minimize damage to the immobilized proteins. The tip deflection−piezo motion calibration was determined from the slope of the constant compliance retraction trace where the tip was in "hard" contact with the surface (i.e., just below turnaround). The spring constant of the cantilevers was ∼0.074 $N \cdot m^{-1}$, as determined by an end-mass resonance technique (*34*). To minimize tip geometry effects, binding measurements were performed with the same tip whenever possible. A minimum of 75 force curves was acquired for a given set of conditions at a given scan rate, repeated on several locations on the substrate. Data analyses were performed using Nanoscope III version 4.22b1 (Digital Instruments, Inc., Santa Barbara, CA) and a program written in our laboratory (SPMCON95) that enables rapid analysis of force curves and compilation of binding forces. However, SPM-

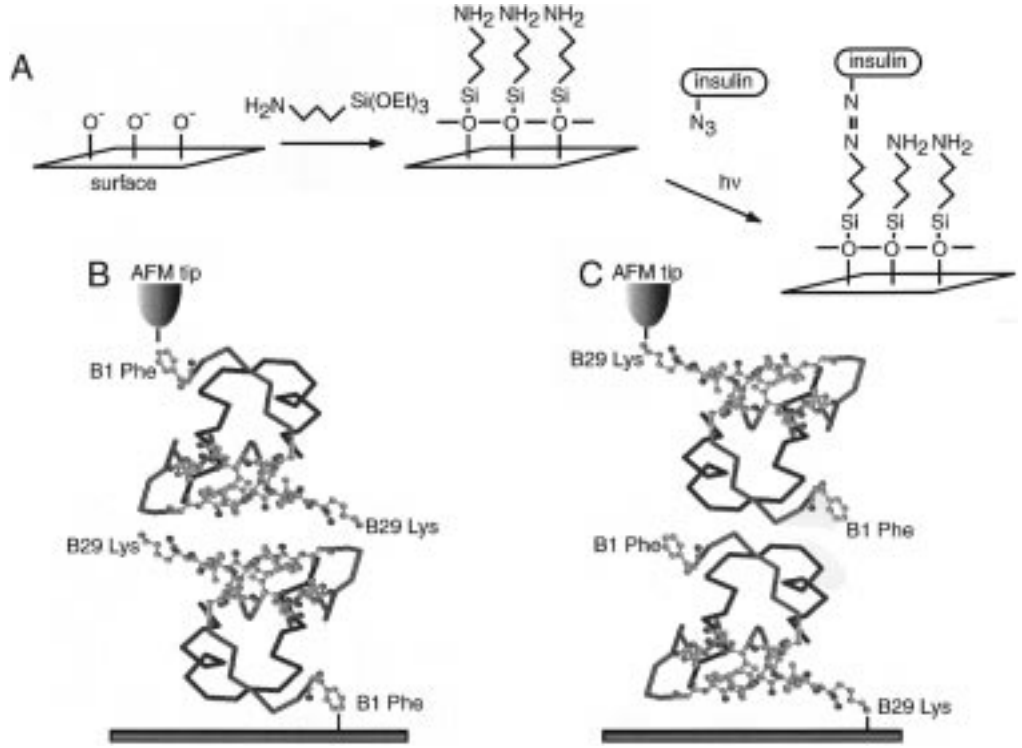

FIGURE 2: (A) Schematic representation of the procedure for anchoring insulin derivatives to substrates. (B, C) Schematic models of idealized oriented insulin monomers immobilized at AFM tips and mica substrates. The insulin monomer is drawn as a backbone model with the A and B chains depicted in blue and red, respectively. Those residues involved in dimer formation as well as the immobilization sites B1 Phe and B29 Lys are depicted as ball-and-stick models. (B) **B1**-MABI functionalized AFM tip and mica substrates. This idealized configuration leaves the binding domains exposed on both the tip and mica surfaces and is denoted as (T)**B1**-MABI:MABI-**B1**(M). (C) **B29**-MABI functionalized AFM tip and mica substrates. This idealized configuration pins the binding domain near the surfaces of the AFM tip and mica substrate and is denoted as (T)**B29**-MABI: MABI-**B29**(M).

CON95 does not automatically detect pull-off events as such detection schemes can fail in the event of multiple unbinding events. Rather, SPMCON95 relies on the user to identify and manually measure unbinding events. Details on the capabilities of SPMCON95, which runs in the Microsoft Windows95 environment, and downloading information can be found on the World Wide Web at http://www.cems.umn.edu/research/ward or at ftp://cyclops.ibme.utoronto.ca.

The influence of various antagonists was examined in succession in the following order: insulin, N-IgG, or MAb 21 using the same tip. Prior to the introduction of a given antagonist, the AFM cell was thoroughly flushed with an aqueous solution containing 6 N urea and 2 N acetic acid to remove the previous antagonist. The AFM cell was refilled with PBS solution and the antagonist solution was introduced via a cannula fitted to the inlet ports of the AFM cell. The total amount of antagonist solution added was approximately 10% of the total AFM liquid cell volume. The irreversibility of Mab 21 binding dictated that this event be performed last in a given series.

The interaction forces were calculated from vertical excursions in the retraction portion of the force curves that were due to sudden unbinding events. The forces associated with the vertical excursions were fitted to a Poisson distribution, with all clearly resolved vertical force excursions above the noise level ~0.03 nN used in the analysis. Histograms of the measured unbinding forces exhibited a highly skewed Poisson distribution as would be expected for a random sampling of a discrete number of events. The average interaction force (F) was estimated from the mean (μ) and variance (σ^2) of each distribution (*35*).

Molecular Simulations. Conformational changes associated with stretching of the insulin dimer were examined using the molecular modeling program Sculpt version 2.5 (Interactive Simulations Inc.; http://www.intsim.com). Molecular models were constructed from the insulin dimer structure reported as the asymmetric unit in the single-crystal X-ray structure of porcine insulin, designated in the Brookhaven Protein Data Bank by entry code pdb4ins. The slight sequence differences between wild-type insulin strains (i.e., human, bovine, or porcine) were ignored.

RESULTS

Imaging of Derivatized Mica Surface. The presence of insulin molecules on the mica surface after photolabeling was verified by tapping mode AFM performed in PBS solution using unmodified AFM tips. AFM of the mica surface after treatment with 3-APTES revealed minor surface roughening (<0.75 nm rms roughness), presumably from polycondensation of this reagent during derivatization (Figure 3A). The surface appeared substantially different after photochemical attachment of the insulin derivatives, exhibiting regular elliptically shaped features (Figure 3B). Image analyses of arbitrarily selected regions of the surface revealed that the height of these features ranged from 2.5 to 2.7 nm. These values are in good agreement with the distance of 2.9 nm between the B1 Phe and B29 Lys residues of the insulin monomer, based on the solution structure of a monomeric insulin mutant as determined by NMR (*27*). The average

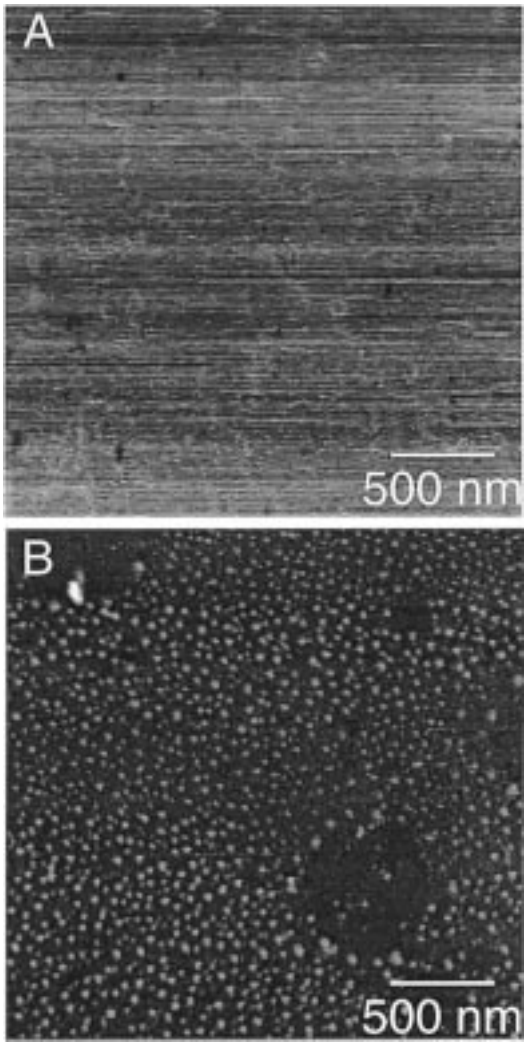

FIGURE 3: Tapping mode AFM images acquired in pH 7.4 PBS buffer solution of mica (A) after treatment with 3-APTES and (B) after photochemical reaction of the surface in panel A with **B29**-MABI. The image in panel B was acquired after copious washing with glycine buffer (pH = 3.5) in order to remove any specifically and nonspecifically bound insulin that was not covalently anchored to the mica surface.

lateral dimensions of the features was 24 nm × 16 nm, which is much larger than expected for an insulin molecule as viewed normal to the binding domain (approximately 3 nm × 2 nm). These overly large dimensions can be attributed to the inherent resolution limits of the AFM tips used in these studies. Larger features (~90 nm × 50 nm) occasionally were observed, possibly due to coupling of photoactive insulin derivatives to covalently anchored insulin monomers. Motion of the attached insulin species on the time scale of AFM imaging also may contribute to an overestimation of the lateral dimensions of these features. The morphology of these insulin-derivatized mica surfaces differed considerably from films of adsorbed insulin on mica, which consisted of randomly oriented aggregates.

The AFM images obtained as described above demonstrate the attachment of insulin molecules to the mica surface. On the other hand, direct verification of the presence of immobilized insulin on the AFM tip cannot be achieved readily by conventional analytical methods owing to the minute amount of insulin on the tip. This difficulty is common to all AFM-based force measurements involving molecules or biomolecules immobilized on the tip. Rather, the presence of insulin on the AFM tip can be inferred from the successful derivatization of the 3-APTES-mica surfaces, as the surface of a Si_4N_3 tip contains native -NH_2 groups and reactive hydroxyl groups capable of reacting with 3-APTES (*36*, *37*). Although the AFM tip was modified with 3-APTES in order to increase the surface density of reactive -NH_2 groups, the low density of active hydroxyl and amino groups on the Si_3N_4 tip and its low radius of curvature would favor the attachment of an insulin monomer on the tip.

Force Measurements. Measurement of intermolecular forces by force microscopy can be performed by monitoring the deflection of an AFM cantilever with a known force constant as a sample surface is moved toward the AFM tip until contact is made and then retracted. Viewed as a Hookian spring, the restoring force (F) of the AFM tip can be estimated as the tip deflection (Δz) multiplied by the (experimentally determined) tip spring constant, k. Once this restoring force exceeds the adhesive force between the tip and sample, a "pull-off" event will occur. The vertical tip jump during pull-off can be used to estimate the interaction force, which can be related to the number of binding sites, adhesive contact area, and the molecular packing density of the bound molecules. Although simplistic in concept, force curves become markedly more complex in the case of biomolecular systems where multiple intermolecular interactions exist and both dissociation and (re)association events may occur on the time scale of the experiment, resulting in broad retraction curves with discrete, possibly quantized, pull-off events. While estimates of the interaction forces may be obtained from the vertical tip jump during pull-off, the width and shape of the retraction curve likely are indicative of processes associated with entropically unfavorable molecular unfolding and elongation. The shape of the retraction curve thus reflects a balance between the competitive entropic and enthalphic processes that are present during association/dissociation.

Force curve measurements performed in buffer solutions at pH 3.5 and 7.5 with bare or 3-APTES-modified AFM tips, and similarly modified mica substrates, were unremarkable, with single sharp unbinding events with negligible jump-to-contact, no discernible hysteresis between the approach and retraction portions of the force curves, and unbinding forces of <0.1 nN. Force curves for an insulin-modified tip and a bare mica surface, a configuration denoted as (T)-**B1**-MABI:(M),[2] in PBS solution (pH = 7.5) also exhibited negligible jump-to-contact, sharp pull-offs, and unbinding forces <0.06 nN (Figure 4A). However, at pH 3.5 in glycine buffer the same configuration exhibited large jump-to-contact and significantly larger binding forces of 4.3 nN (Figure 4B), consistent with strong electrostatic interactions between the negatively charged bare mica surface and the positively charged insulin molecule at this pH, which is below the isoelectric point of insulin (pI = 6.4) (*38*). These observa-

[2] The configuration of a given experiment is denoted such that the residue bound to the AFM tip (T) or mica (M) is indicated in boldface type adjacent to the respective surfaces. For example, (T)**B1**-MABI:MABI-**B29**(M) refers to the configuration in which an insulin molecule is immobilized on the tip via the B1 Phe residue while the mica-bound insulin molecule is tethered via the B29 Lys residue.

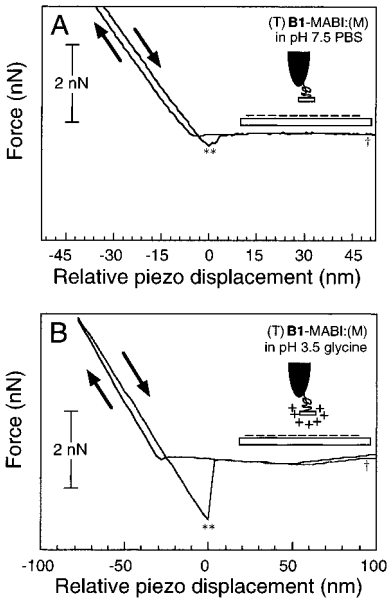

FIGURE 4: Representative force curves for (T)**B1**-MABI:(M) acquired at a scan rate of 0.5 Hz in (A) pH = 7.5 PBS and (B) pH = 3.5 glycine buffer solutions. The curves illustrate the deflection of the AFM tip as the tip approaches the sample surface (left-facing arrow) and is retracted from the surface (right-facing arrow). The *x*-axis is defined as the sample surface displacement relative to the minimum in the retraction portion of the force curve. The *y*-axis is defined by the neutral tip position (†) when the tip is no longer in contact with the surface. The inset schematics depict the interaction between a tethered insulin molecule at an AFM tip and the negatively charged mica surface. In panel A, the solution pH > p$I_{insulin}$ and the insulin molecule remains nominally neutrally charged, whereas in panel B, the solution pH < p$I_{insulin}$ and the insulin molecule is positively charged. Adhesive forces are determined from the retraction portion of the force curve when a "pull-off" event occurs (**) and are calculated from the vertical tip jump († − **). These data clearly indicate stronger binding in the acidic buffer solution where the pH is below the isoelectric point of insulin (pI ∼ 6.4).

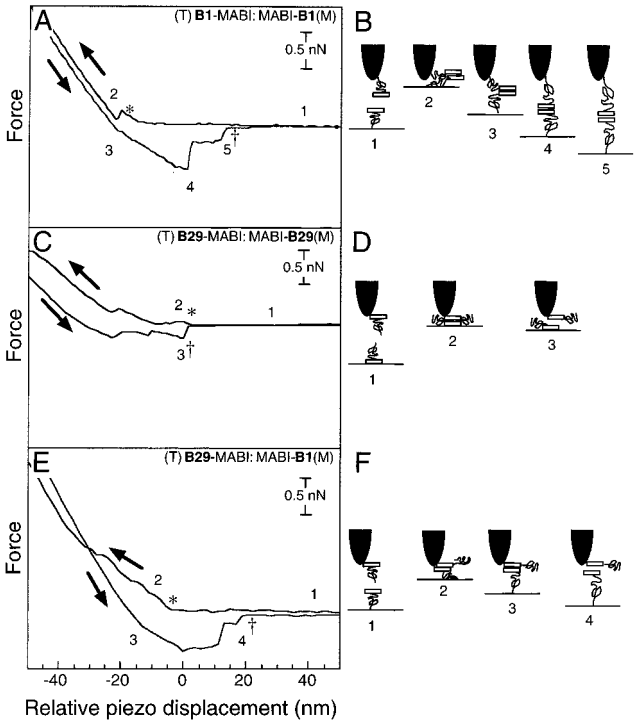

FIGURE 5: Representative force curves acquired in pH 7.5 PBS buffer at a scan rate of 0.5 Hz with a corresponding schematic representation of insulin monomer elongation and interface distortion for each. (A, B) (T)**B1**-MABI:MABI-**B1**(M) exhibits a broad retraction curve prior to well-defined multiple unbinding events. (C, D) (T)**B29**-MABI:MABI-**B29**(M) exhibits repulsive forces between the tip and substrate on tip approach, signifying unfavorable insulin molecule conformations for dimer formation, as compared with the behavior suggested by the smooth approach curve seen in panel A. In panels A and B, an asterisk denotes onset of repulsive tip−sample forces, and a dagger denotes return to nominally zero tip deflection. (E, F) Force curve for (T)**B1**-MABI:MABI-**B29**(M). Note that the final unbinding distance for panel A, as measured from the global minimum, is approximately twice that of panel E. In panels B, D, and F the rectangles denote the B29 Lys residues located in the insulin dimerization domain. The numbers on the force curves correspond to the position of the tip illustrated in the schematic representations.

tions argue that the photoreactive insulin derivative was anchored to the AFM tip.

In contrast to the configuration (T)**B1**-MABI:(M), force curves for the configuration (T)**B1**-MABI:MABI-**B1**(M) in which insulin was immobilized via the B1 Phe residue on both the AFM tip and the mica surface exhibited pronounced hysteretic behavior during retraction of the sample from the tip (Figure 5). The adhesion force during retraction increased monotonically to a global minimum, which was located beyond the point of initial repulsive contact observed during the approach curve. At distances beyond this minimum the force curves typically exhibited multiple vertical jumps, usually separated by regions of near zero slope. Force curves with the same qualitative features were repeatedly obtained on the same region, indicating that the protein was robust under the conditions of measurement. A representative force curve is shown in Figure 5A. These features are similar to those observed in force curves for other biomolecular systems (*10*−*15*). In our case, the featureless broad region of the retraction curve between the repulsive onset and the global minimum is presumed to result from nonspecific adhesion forces between entangled insulin chains of the opposing surfaces. The vertical jumps immediately following the minimum suggest sudden unbinding of intermolecular bonds between residues across the dimerization interface. The regions of near horizontal slope indicate minimal tip deflection as the tip−sample separation is increased, suggesting extension of the dimerized insulin molecules due to mechanically induced protein unfolding. Our analyses included all unbinding events that immediately followed the global minimum of the retraction curve (denoted as 3 in Figure 5) above the noise level of our instrument. Figure 5B graphically depicts these considerations. Histograms of the measured unbinding forces exhibited a highly skewed Poisson distribution, as expected for a random sampling of a discrete number of events (Figure 6). While previous measurements of ligand−receptor binding have relied on the direct determination of the unbinding force from the magnitude of the final vertical jump observed in the retraction portion of the force curve (*13*−*15*), we were unable to analyze binding forces from the final insulin monomer−monomer unbinding events as the final vertical excursions were difficult to distinguish from instrument noise, making the choice of the final unbinding event somewhat subjective and arbitrary. Consequently, autocorrelation analysis using data acquired in this manner were inconclusive and unbinding events could not be quantified by this approach. Rather, we determined an average interaction force (F) from the ratio of the variance (σ^2) to the mean (μ) of the measured forces. The average

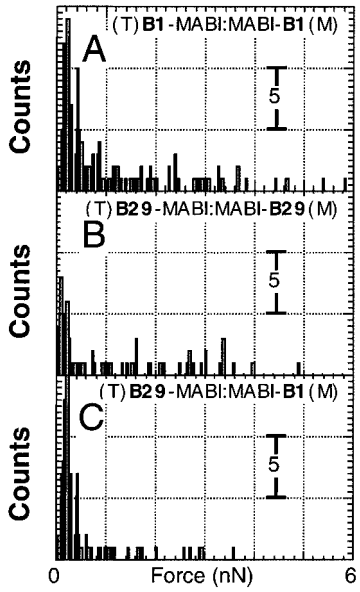

FIGURE 6: Histograms of unbinding forces for (A) (T)**B1**-MABI:MABI-**B1**(M), (B) (T)**B29**-MABI:MABI-**B29**(M), and (C) (T)**B29**-MABI:MABI-**B1**(M) interactions. All data were from force curves performed in pH 7.5 PBS buffer at a scan rate of 0.5 Hz. The histograms reveal a skewed Poisson distribution of forces with a substantial reduction in the number of unbinding events and their forces depending on the orientation of the bound insulin molecules.

binding force for the (T)**B1**-MABI:MABI-**B1**(M) configuration, determined by analysis of numerous force curves acquired at a retraction rate of 100 nm·s^{-1}, was 1.34 nN (Table 2).

Extensional unfolding of the insulin molecules was corroborated by force measurements performed with other insulin−insulin configurations. The average interaction force measurement for the (T)**B29**-MABI:MABI-**B29**(M) configuration, in which the insulin molecules are tethered by the B29 Lys group to the tip and mica surfaces, was comparable to that measured for (T)**B1**-MABI:MABI-**B1**(M) (Table 2). However, the shape of the force curves for the (T) **B29**-MABI:MABI-**B29**(M) configuration as shown in Figure 5C differed dramatically as the retraction curve returns to zero deflection at the onset of repulsion, in contrast to the long unbinding distance observed for the (T)**B1**-MABI:MABI-**B1**(M) configuration. This contrasting behavior can be explained by the different position of the binding domain with respect to the tip and mica surfaces as depicted in Figure 5D. In the (T)**B29**-MABI:MABI-**B29**(M), the binding domain is essentially pinned at the tip surface; dimer rupture can occur but extensional unfolding is not possible. Furthermore, the unbinding distances observed for the (T)**B1**-MABI:MABI-**B29**(M) configuration (Figure 5E), which exhibited an average interaction force of 0.96 nN (Table 2), were roughly half that observed for (T)**B1**-MABI:MABI-**B1**(M). This is to be expected if only one binding site is pinned at the surface as illustrated in Figure 5F. In contrast, the binding domain in the (T)**B1**-MABI:MABI-**B1**(M) configuration is distal from the anchoring residue on both surfaces, which allows extensional unfolding of the insulin molecule as long as the monomer−monomer interface remains intact.

To demonstrate the specificity of the force measurement, we examined the effect of adding insulin or insulin antibodies. Average interaction forces obtained under these conditions are presented in Table 2. The addition of insulin to the AFM cell configured with either (T)**B1**-MABI:MABI-**B1**(M) or (T)**B29**-MABI:MABI-**B29**(M) decreased the binding forces by about 35% and 23%, respectively. This process was reversible as the original force curves were obtained after the dissociation of dimers by washing with an aqueous solution containing 6 M urea and 2 M acetic acid. The force curves measured for the (T)**B1**-MABI:MABI-**B1**(M) configuration after the addition of a monoclonal anti-insulin antibody MAb 21, which is directed specifically against an insulin epitope encompassing most of the insulin dimer-forming residues *(34)*, exhibited negligible adhesive unbinding forces (<0.03 nN). In contrast, force curves of the (T)**B29**-MABI:MABI-**B29**(M) configuration obtained in the presence of this antibody were highly variable, with no consistent effect of the antibody on the binding events. Control experiments in which force curves were obtained in the presence of N-IgG revealed a reduction in binding forces for the (T)**B1**-MABI:MABI-**B1**(M) configuration but an increase for the (T)**B29**-MABI:MABI-**B29**(M) configuration, in contrast with the MAb 21 results.

DISCUSSION

Insulin−Insulin Association. In the present study, we have used force microscopy to evaluate interactions between oriented insulin molecules. Force curves measured between insulin covalently bound to force microscope tips and silane-modified mica revealed trends in retraction curve shapes consistent with the orientation of the tethered-insulin molecules. Specifically, extensional unfolding was most prevalent when the insulin molecules were oriented to favor dimer formation. When measured from the global minimum of the retraction portion of the force curves, these unbinding distances approach 20 nm, with occasional values approaching 40 nm. In this study we have chosen to measure the unbinding distance from the global minimum rather than the apparent onset of repulsion (asterisks in Figure 5), which can be attributed to contact between the hard surfaces of the mica and the AFM tip following interpenetration and entanglement of opposing insulin molecules. As the mica surface is retracted, the tip will disengage from the mica. However, nonspecific interactions between the entangled insulin chains will cause the observed hysteresis and the broad monotonic increase in adhesion force. This disentanglement also will contain entropic contributions due to conformational changes required for this process. Eventually the tip will be retracted so that the insulin chains are disentangled and the dimerization interface is nominally parallel to the planes of the opposing surfaces with the opposing monomers in an unstretched, near-native conformation. Further retraction will lead to the first unbinding event, thereby establishing the global minimum. Consequently, insulin extension and the distance at which complete rupture of the dimerization interface occurs are better measured from the global minimum rather than the onset of hard repulsive contact. These unbinding events will occur when the entropic penalty of unfolding exceeds the bond strength of a given set of intermolecular interactions.

A similar model was proposed in an AFM study of Fab−anti-human serum albumin interactions. These studies, which extended the ligands away from the tip and sample surface with flexible poly(ethylene glycol) tethers, revealed

Table 2: Interaction Forces between Functionalized AFM Tips and Substrates in pH 7.5 PBS Solution at a Scan Rate of 0.5 Hz

tip modification	mica derivatization	binding antagonist	average binding force[a] (nN)	variance (σ) (nN)
(T)**B1**-MABI	none	none	0.06	
(T)**B1**-MABI	MABI-**B1**(M)	none	1.34	1.4
(T)**B1**-MABI	MABI-**B1**(M)	insulin	0.88	0.62
(T)**B1**-MABI	MABI-**B1**(M)	N−IgG	0.29	0.15
(T)**B1**-MABI	MABI-**B1**(M)	MAb-21	<0.03[b]	0
(T)**B29**-MABI	MABI-**B29**(M)	none	1.35	1.58
(T)**B29**-MABI	MABI-**B29**(M)	insulin	1.04	1.38
(T)**B29**-MABI	MABI-**B29**(M)	N−IgG	1.55	0.98
(T)**B29**-MABI	MABI-**B29**(M)	MAb-21	*c*	

[a] The average binding forces were calculated by fitting a Poisson distribution to the forces measured for distinct vertical unbinding events. [b] No measurable forces. [c] The force curves for (T)**B29**-MABI:MABI-**B29**(M) in the presence of MAb 21 were very erratic, precluding acquisition of interaction forces and determination of a binding force.

that dissociation occurred once the tethers had become extended, suggesting that the association forces binding the Fab complex were stronger than the conformational constraints on the tethers (*10*). Similar molecular elongation phenomena have been reported in optical trap studies of DNA extensibility (*39*, *40*) and AFM studies of the forced unfolding of titin IgG domains (*41*), tethered duplex DNA (*42*), the shear-induced elongation of human von Willebrand factor (*43*), and the unbinding of complementary DNA sequences (*15*).

The occasional observation of unbinding distances that exceeded 20 nm may be due to oligomers formed by photocross-linking of a photoreactive insulin monomer to a surface-immobilized insulin monomer during surface immobilization. These oligomers would still expose a binding domain to an approaching insulin monomer and comparable binding forces would be expected, with the apparent extensional length increased by a factor proportional to the number of insulin molecules in the oligomer. The occasionally observed unbinding distance of 40 nm would be consistent with an oligomer of two insulin molecules. The long unbinding distance also may be due to elongation of a polymeric silane layer formed by siloxane cross-linking during surface modification with 3-APTES. However, it has been shown through AFM studies that lateral forces in excess of 300 nN (using unmodified cantilevers similar to the type used in the present study) are required to disrupt such siloxane layers from the mica surface (*44*). These data argue against the interpretation that the unbinding forces observed in our present study represent contributions from a polymeric silane layer.

The unbinding distances observed here suggest substantial unfolding and "mechanical denaturation" of the insulin molecule during retraction. Since force curves obtained repeatedly on the same region were nominally identical, it is unlikely that irreversible changes in the binding domains occurred during repeated force measurements. Indeed, molecular dynamics simulations have demonstrated that the insulin molecule is inherently flexible (*45*), which is believed to be important for insulin receptor binding (*46*). While studies of native insulin folding and unfolding are hindered by its self-association properties, necessitating the use of insulin analogues that exist as monomers (*47*, *48*), previous stopped-flow studies of protein refolding suggest that a protein's native β-structure is formed within a few milliseconds of the initiation of the refolding reaction (*49*). These data argue that insulin refolding likely occurs within the time frame (order of seconds) of the AFM force experiment and that sequential force curve measurements are acquired with insulin monomers that have reestablished their native conformation after dimer dissociation. Similar effects were observed in force microscopy studies of titin immunoglobulin domain unfolding and apparent refolding (*42*).

To determine the feasibility of extensional unfolding prior to dimer rupture, the retraction portion of the force curve beyond the disentanglement regime was simulated computationally by pulling on the B1 Phe terminus located at the opposite ends of an insulin dimer. Dissociation of the streptavidin−biotin complex was simulated by molecular dynamics in an analogous fashion (*50*). The conformation of the model during each step of the simulation was determined by local minimization of the model's potential energy including contributions from torsion, van der Waals, hydrogen-bonding, and electrostatic interactions (*51*). The forces applied at the B1 Phe termini were propagated through changes in secondary structure with rigid constraints applied to bond lengths, bond angles, and planar groups. No other constraints on chain conformation or residue orientations were imposed. The simulations revealed that the interface between the two insulin monomers, based on the crystallographic dimer, which is held together by numerous hydrophobic, hydrogen-bonding, and aromatic interactions, retains its structure and conformation as forces are applied nominally perpendicular to the interface (Table 1). In particular, the simulations revealed that as the external forces were applied, the interchain A7−B7 and A20−B19 disulfides, and the intrachain A6−A11 disulfide remained intact and the (1 → 4) β-turn defined by residues B20−23 in the insulin monomer became significantly distorted, with the B chain adopting a nearly fully extended conformation in the B1−B20 region prior to rupture of the monomer−monomer interface. In such an orientation, the distance between opposing B1 Phe residues across the monomer−monomer interface increased to nearly 20 nm prior to rupture. Although simulations cannot approach the AFM time scale owing to computational limitations, these results suggest that the intrachain interactions dictating the native B chain conformation are weaker than forces acting across the monomer−monomer interface and provide a conceptual basis for the apparent extensibility of the insulin dimer prior to disruption.

As suggested by earlier AFM force measurement studies of the unbinding between biotin and a series of avidin mutants, the contribution of factors such as entropically driven ligand binding remains unclear (*53*). It is likely such considerations apply to conformationally flexible complexes

such as insulin, which comprise numerous interactions and a high degree of rotational freedom. In the case of protein−protein interactions, the measured adhesion force reflects a distribution of interactions and bond energies between different functional groups on different residues rather than a single defining interaction force (*52, 53*). We attribute the failure of autocorrelation analysis in our studies of insulin dimerization to these considerations. This prompted us to evaluate the unbinding forces by Poisson statistics, which do not rely on the resolution of binding force quanta. Used previously to determine single-bond forces resulting from van der Waals and hydrogen-bonding interactions (*35*), this approach is appropriate for a system in which the adhesion force is the sum of a finite number of discrete bonds that act independently of each other (this last point may be debated owing to the cooperative nature of protein interactions).

The magnitude of insulin−insulin interaction forces was approximately 1.34−1.35 nN regardless of the orientation of the insulin monomers, which is larger than that observed for binding between streptavidin and biotin (0.26 nN) (*54*) and human serum albumin and its polyclonal antibody *(55*) but comparable to forces reported for the interaction between complementary 20 base-pair DNA strands (1.52 nN) (*15*). However, care must be exercised when comparing unbinding forces measured for different systems; these forces not only reflect thermodynamic differences and the initial contact force (*11*) but also may be rate-dependent owing to differences in kinetics of bond breaking, bond formation, and conformational relaxation during retraction (*35*). As reported by others (*56*, *57*), the AFM force measurement relies on a constant rate of tip (or substrate) retraction. Thus the AFM tip applies a time-dependent restoring force, $F_r(t) = k\Delta z/\Delta t$, which suggests that the observed dissociation force is convoluted with the *rate* of retraction and thus may not be a true measure of individual bond strengths. Indeed, our studies revealed that the number of "unbinding events" decreased with increasing retraction rate accompanied by a relatively minor increase in the unbinding force per event. Similar effects were observed in an AFM study of titin unfolding (*42*) and a molecular dynamics simulation of streptavidin−biotin dissociation (*46*). Although it is possible to minimize tip velocities, this in turn raises issues of electronic noise and instrument stability.

The complex structure of the insulin monomer binding interface precludes the use of partial blocking strategies such as those employed by others in studies of (strept)avidin−biotin binding (*13*, *14*). For the present study, it clearly is more appropriate to measure the intermolecular binding forces in the presence of reagents specifically designed to inhibit insulin−insulin self-association. We addressed this by measuring insulin interaction forces in the presence of soluble insulin or anti-insulin antibodies. The introduction of soluble insulin did result in significant reductions in the measured interaction forces. However, the interpretation of these findings is complicated by both specific and nonspecific interaction of the soluble insulin with insulin anchored on the mica and on the tip. The monoclonal antibody MAb 21, directed at an epitope in the dimerization domain of insulin, clearly prevented dimer formation in the (T)**B1**-MABI:MABI-**B1**(M) configuration, as evidenced in the consistent lack of unbinding events during tip retraction. In the case of the (T)**B29**-MABI:MABI-**B29**(M) configuration, erratic force curves were obtained, suggesting nonspecific interactions of the antibody with the oriented insulin. We propose that the complexation of MAb 21 with (T/M)**B29**-MABI may be weak due to poor accessibility of the epitope. Occasional dissociation of the weak complex would reexpose the insulin so that dimer formation can be detected on the time scale of the AFM experiment (∼seconds between consecutive force curves). The problem of using antibodies as specific blocking agents also was demonstrated by unbinding force measurements performed in the presence of N−IgG. This antibody should show no specificity to the immobilized insulin molecules; however, we observed a reduction in the (T)**B1**-MABI:MABI-**B1**(M) binding force but an increase in the (T)**B29**-MABI:MABI-**B29**(M) binding force.

We note several key issues regarding the measurement of forces between large conformationally flexible proteins. Specifically, a valid concern is whether the measured forces reflect *single* molecule−molecule interactions as it is difficult to control the density of immobilized molecules, especially at the surface of the AFM tip. Furthermore, it is difficult to conclusively identify the conformation of the tethered molecules and that it is likely that a distribution of molecular orientations exist within the constraints dictated by the tether point. In the present study, this would reflect the mobility of the insulin monomer relative to either B1 Phe or B29 Lys. Moreover, the functional complexity of a protein would dictate the presence of adhesive interactions regardless of the orientation of the protein. To address these concerns, which are intrinsic to these types of force measurements, we considered the following. The specificity of the binding process is reflected in the width and depth of the retraction portion of the force curve and not solely in the absolute magnitude of the observed unbinding forces. Thus, it is reasonable to expect that when the tethered insulin molecules are oriented properly for dimer formation to occur, the accompanying higher binding forces and elongation events would be reflected in a broader and deeper retraction force curve well. Such favorable interactions need not be formed during tip approach but may also result from rearrangement of the molecules during tip retraction. It is therefore necessary to examine carefully the shape of both the approach and retraction portions of the force curves in order to correctly evaluate the unbinding events. We propose that such effects are largely accounted for in statistical analyses of the unbinding events as nonspecific interactions and would not give rise to statistically relevant unbinding events, except in the unlikely event of simultaneous rupture of all specific and nonspecific intermolecular bonds. Background nonspecific protein−protein and protein−surface interactions also bear consideration. In our studies, experiments performed with **B1**-MABI- or **B29**-MABI-modified AFM tips and mica modified with *nonspecifically adsorbed* insulin (or anti-insulin antibodies) revealed highly erratic retraction curves with minimal ∼0.07 nN unbinding, comparable to the force curves acquired between **B1**-MABI- or **B29**-MABI-modified AFM tips and bare mica (data not shown). These results support that the measured insulin monomer−monomer interaction forces and observed retraction force curve well shapes reflect the *relative* freedom of the insulin dimerization

binding domain as dictated by the location of the tethering site.

These studies demonstrate that specific protein−protein interaction forces, the effect of molecular orientation on these forces, and the influence of antagonists can be studied with high resolution by AFM. Our data revealed that insulin dimer unbinding occurs near the limit of extensibility of the insulin B-chain with rupture of specific hydrogen-bonding and hydrophobic interactions acting across the dimer interface. The extent of insulin extensibility was found to depend on the proximity of the immobilization anchor to the insulin dimer binding domain, a notion corroborated by molecular simulations of the unbinding process. Furthermore, our data illustrate the complexity of measuring protein−protein interactions by AFM and, in the case of insulin, that the observed unbinding forces are likely very sensitive to interface geometry, structure, and residue conformations. The final unbinding event observed in force curves, while likely due to the unbinding of a specific residue or group of residues, may not thus be characteristic of the overall unbinding force**.** Nevertheless, the influence of antagonists, particularly a monoclonal antibody directed against the insulin dimerization binding domain, can be examined directly with AFM force measurements. The possibility of attaching photoactive groups to other protein molecules suggests a useful strategy for examining the effect of sequence alterations and binding site modifications on interaction forces, while the in situ nature of AFM force measurements renders it ideally suited for characterizing the effect of solution conditions, such as pH and ionic strength, on protein−protein interactions. Although AFM force measurements are inherently complex, we anticipate that this and related approaches will facilitate elucidation of antigen−antibody, protein−protein, and protein−receptor interaction forces and energies, as well as the development of therapeutic protein formulations.

ACKNOWLEDGMENT

We gratefully acknowledge Dr. Alex Marks of the Banting and Best Department of Medical Research, University of Toronto, for making available the hybridoma producing the monoclonal anti-insulin antibody, MAb 21, used in these studies. We thank Drs. Michael R. DeFelippis and John M. Beals, Eli Lilly and Company, for useful discussions.

REFERENCES

1. Helm, C. A., Knoll, W., and Isrealachvili, J. N. (1991) *Proc. Natl. Acad. Sci. U.S.A. 88*, 8169.
2. Kuo, S. C., and Sheetz, M. P. (1993) *Science 260*, 232.
3. Thomas, R. C., Houston, J. E., Crooks, R. M., Kim, T., and Michalske, T. A. (1995) *J. Am. Chem. Soc. 117*, 3830.
4. Boland, T., and Ratner, B. D. (1995) *Proc. Natl. Acad. Sci. U.S.A. 92*, 5297.
5. Evans, E., Ritchie, K., and Merkel, R. (1995) *Biophys. J. 68*, 2580.
6. Frisbie, C. D., Rozsnyai, L. F., Noy, A., Wrighton, M. S., and Lieber, C. M. (1994) *Science 265*, 2071.
7. Meyer, G., and Amer, N. M. (1988) *Appl. Phys. Lett. 53*, 1045.
8. Williams, J. M., Han, T., and Beebe, T.P., Jr. (1996) *Langmuir 12*, 1291.
9. Ohnesorge, F. and Binnig, G. (1993) *Science 260*, 1451.
10. Hinterdorfer, P., Baumgartner, W., Gruber, H. J., Schilcher, K., and Schindler, H. (1996) *Proc. Natl. Acad. Sci. U.S.A. 93*, 3477.
11. Allen, S., Chen, X., Davies, J., Davies, M. C., Dawkes, A. C., Edwards, J. C., Roberts, C. J., Sefton, J., Tendler, S. J. B., and Willimans, P. M. (1997) *Biochemistry 36*, 7457.
12. Lee, G. U., Kidwell, D. A., and Colton, R. J. (1994) *Langmuir 10*, 354.
13. Florin, E. L., Moy, V. T., and Gaub, H. E. (1994) *Science 264*, 415.
14. Moy, V. T., Florin, E. L., and Gaub, H. E. (1994) *Science 266*, 257.
15. Lee, G. U., Chrisey, L. A., and Colton, R. J. (1994) *Science 266*, 771.
16. Webster, D. M., Henry, A. H., and Rees, A. R. (1994) *Curr. Opin. Struct. Biol. 4*, 123.
17. Ito, Y., Zheng, J., Imanishi, Y., Yonezawa, K., and Kasuga, M. (1996) *Proc. Natl. Acad. Sci. U.S.A. 93* (8), 3598.
18. Horwitz, J. I., Toner, M., Tompkins, R. G., and Yarmush, M. L. (1993) *Mol. Immunol. 30*, 1041.
19. Chiet, L., and Wolf, F. J. (1964) *Arch. Biochem. Biophys. 106*, 1.
20. Weber, P. C., Ohlendorf, D. H., Wendoloski, J. J., and Salemme, F. R (1989) *Science 343*, 85.
21. Green, N. M. (1990) *Methods Enzymol. 184*, 51.
22. Brange, J., Owens, D., Kang, S., and Volund, A. (1990) *Diabetes Care 13*, 923.
23. Wood, S. P., Blundell, T. L., Wollmer, A., Lazarus, N. R., and Neville, R. W. J. (1975) *Eur. J. Biochem. 55*, 531.
24. Baker, E. N., Blundell, T. L., Cutfield, J. F., Cutfield, S. M., Dodson, E. J., Dodson, G. G., Hodgkin, D. M. C., Hubbard, R. S., Isaacs, N. W., Reynolds, C. D., Sakabe, K., Sakabe, N., and Vijayan, N. M. (1988) *Philos. Trans. R. Soc. London 319*, 369.
25. Blundell, T., Dodson, G., Hodgkin, D., and Mercola, D. (1972) *Adv. Protein Sci. 26*, 280.
26. Pekar, A. H., and Frank, B. H. (1972) *Biochemistry 11*, 4013.
27. Kaarsholm, N. C., and Ludvigsen, S. (1995) *Receptor 5*, 1.
28. Yip, C. C., Yeung, C.W. T., and Moule, M. L. (1980) *Biochemistry 19*, 70.
29. Kurth, D. G., and Bein, T. (1993) *Langmuir 9*, 2965.
30. Iler, R. K. (1979) *The Chemistry of Silica*, Wiley and Sons, New York.
31. Vinckier, A., Heyvaert, I., D'Hoore, A., McKittrick, T., Van Haesendonck, C., Engelborghs, Y., and Hellemans, L. (1995), *Ultramicroscopy 57*, 337.
32. Marks, A., Yip, C., and Wilson, S. (1985) *Mol. Immunol. 22* (3), 285.
33. Yip, C. C., and Logothethopoulos, J. (1969) *Proc. Natl. Acad. Sci. U.S.A. 66*, 2415.
34. Cleveland, J. P., Manne, S., Bocek, D., and Hansma, P. K. (1993) *Rev. Sci. Instrum. 64*, 403.
35. Evans, E., Berk, D., and Leung, A. (1991) *Biophys. J. 59*, 838.
36. Senden, T. J., Drummond, C. J., and Kekicheff, P. (1994) *Langmuir 10*, 358.
37. Bergstrom, L., and Bostedt, E. (1990) *Colloids Surf. 49*, 183−197.
38. Kaarsholm, N. C., Havelund, S., and Hougaard, P. (1990) *Arch. Biochem. Biophys. 283*, 496.
39. Cluzel, P., Lebrun, A., Heller, C., Lavery, R., Viovy, J. L., Chatenay, D., and Caron, F. (1996) *Science 271*, 792.
40. Smith, S. B., Cui, Y., and Bustamante, C. (1996) *Science 271*, 795.
41. Rief, M., Gautel, M., Oesterhelt, F., Fernandez, J. M., and Gaub, H. E. (1997) *Science 276*, 1109.
42. Noy, A., Vezenov, D. V., Kayyem, J. F., Meade, T. J., and Lieber, C. M. (1997) *Chem. Biol. 4* (7), 519.
43. Siedlecki, C. A., Lestini, B. J., Kottke-Marchant, K., Eppell, S. J., Wilson, D. L., and Marchant, R. E. (1996) *Blood 88* (8), 2939.
44. Xiao, X.-D., Liu, G.-Y., Charych, D. H., and Salmeron, M. (1995) *Langmuir 11*, 1600.
45. Mark, A. E., Berendsen, H. J. C., and van Gunsteren, W. F. (1991) *Biochemistry 30*, 10866.
46. Engels, M., Jacoby, E., Krüger, P., Schlitter, J., and Wollmer, A. (1992) *Protein Eng. 5* (7), 669.

47. Bryant, C., Strohl, M., Green, K., Long, H. B., Alter, L. A., Pekar, A. H., Chance, R. E., and Brems, D. N. (1992) *Biochemistry 31*, 3692.
48. Brems, D. N., Brown, P. L., Hekenlaible, L. A, and Frank, B. H. (1990) *Biochemistry 29*, 9289.
49. Ptitsyn, O. B. (1994) *Protein Eng. 7* (5), 593.
50. Grubmüller, H., Heymann, B., and Tavan, P. (1996) *Science 271*, 997.
51. Surles, M. C., Richardson, J. S., Richardson, D. C., and Brooks, F. P., Jr. (1994) *Protein Sci. 3*, 198.
52. Pierres, A., Benaliel, A.-M., Bongrand, P., and van der Merwe, P. A. (1996) *Proc. Natl. Acad. Sci. U.S.A. 93*, 15114.
53. Bruinsma, R. (1997) *Proc. Natl. Acad. Sci. U.S.A. 94*, 375.
54. Chilkoti, A., Boland, T., Ratner, B. D., and Stayton, P. S. (1995) *Biophys. J. 69*, 2125.
55. Dammer, U., Hegner, M., Anselmetti, D., Wagner, P., Dreier, M., Huber, W., and Güntherodt, H.-J. (1996) *Biophys. J. 70*, 2437.
56. Evans, E., and Ritchie, K. (1997) *Biophys. J. 72*, 1541.
57. Izrailev, S., Stepaniants, S., Balsera, M., Oono, Y., and Schulten, K. (1997) *Biophys. J. 72*, 1568.

BI9722756